J|A|C|S
ARTICLES
Published on Web 06/05/2007

Metallic versus Covalent Bonding: Ga Nanoparticles as a Case Study

Paolo Ghigna,*,† Giorgio Spinolo,†,⊥ Giovanni Battista Parravicini,‡ Angiolino Stella,‡ Andrea Migliori,§ and Richard Kofman||

Contribution from the INSTM, IENI/CNR, Dipartimento di Chimica fisica M. Rolla, Università di Pavia, I27100 Pavia, CNISM, Dipartimento di Fisica A. Volta, Università di Pavia, I27100 Pavia, Italy, LAMEL/CNR, I 40129 Bologna, Italy, [4] LPMC, Université de Nice-Sophia Antipolis, CNRS UMR 6622, 06108 Nice Cedex 2, France, and IUSS, I27100 Pavia, Italy

Received January 27, 2007; E-mail: paolo.ghigna@unipv.it

Abstract: A systematic X-ray absorption spectroscopy investigation of the local coordination in gallium nanostructures has been performed as a function of temperature and particle size. It is shown that the nanostructure strongly affects the polymorphism of solid gallium and the (meta)stability range of the liquid phase (in agreement with previous works) and that the surface tension acts in the same direction as hydrostatic pressure in stabilizing the Ga solid phases. The effect of surface free energy is first to favor the metallic arrangement of the δ phase and then to stabilize a liquid-like phase based on dimeric molecules even at 90 K. The Ga−Ga distance in the dimers is lower in the liquid phase than in the α solid. The experimental results are discussed in comparison with molecular dynamic calculations to assess the presence of *covalent* character of the dimeric Ga_2 units in liquid nanostructured gallium.

1. Introduction

Interest toward the chemistry of elemental gallium arises for many, variously related aspects. The density of the liquid higher than that of the main solid phase (α) places Ga into the minority set of substances that show increasing stability of the liquid with increasing pressure and generically indicates an anomalous bonding behavior with respect to other metals. α-Gallium is indeed a very particular metal made of diatomic units with a marked pseudogap in the density of states at the Fermi level and strongly anisotropic electronic conductivity. In spite of its high reactivity with oxygen, Ga is indeed a nice experimental model for investigating the properties of liquid metals particularly because the α crystal melts slightly above room temperature (303 K). The element, however, shows a complex polymorphism that has been deeply investigated experimentally and computationally:[1−4] the other crystalline phases have significantly different structures based on different local arrangements and building units, which are made, for instance, of zigzag chains of atoms (β phase) or five different coordination environments (δ phase). Remarkably, these crystal structures do not show the "anomalous" properties of α-Ga.

The bonding behavior can also be affected by the additional free energy contribution occurring at a phase boundary. In simple words and using the naïve language of the dangling bonds model, the interfacial region is expected to be richer, with respect to bulk, in the species that show less strong bonds among each other. For gallium, this picture suggests preference for a structure based on dimeric units, where the weak bonds between units are broken at the interface while the strong bond within a single unit is retained. On the experimental side, we can recall that STM investigations of the (001) surface of α-Ga have shown wide atomically flat terraces, and an analysis of the step-height distribution revealed no monoatomic steps,[5] while a diamond single-crystal surface has been shown[6] to strongly orient the Ga dimers. Computationally, different results have been obtained[7,8] with different crystallographic surfaces: while the (001) surface shows a complex structure with strong reconstruction, the (010) structure is made of dimers oriented out of the surface by $\sim$17°.

Evidence of the influence of interfaces on Ga bonding is also given by a large amount of experiments available from recent or older literature[9−14] on the effect of confinement on gallium

† Dipartimento di Chimica fisica *M. Rolla*, Università di Pavia.
‡ Dipartimento di Fisica *A. Volta*, Università di Pavia.
§ LAMEL/CNR.
|| Université de Nice.
⊥ IUSS.

(1) Bernasconi, M.; Chiarotti, G. L.; Tosatti, E. *Phys. Rev. B* **1995**, *52* (14), 9988−9998.
(2) Comez, L.; Di Cicco, A.; Itié, J. P.; Polian, A. *Phys. Rev. B* **2005**, *65* (1), 014114-1−014114-10.
(3) Defrain, A. *J. Chim. Phys. Phys.-Chim. Biol.* **1977**, *74* (7−8), 851−862.
(4) Bosio, L.; Defrain, A.; Epelboin, I. *J. Physiol. (Paris)* **1966**, *27* (1−2), 61−71.
(5) Züger, O.; Dürig, U. *Phys. Rev. B* **1992**, *46* (11), 7319−7321.
(6) Huisman, W. J.; Peters, J. F.; Zwanenburg, M. J.; de Vries, S. A.; Derry, T. E.; Abernathy, D.; van der Veen, J. F. *Nature* **1997**, *390*, 379−381.
(7) Bernasconi, M.; Chiarotti, G. L.; Tosatti, E. *Phys. Rev. Lett.* **2007**, *70* (21), 3295−3298.
(8) Bernasconi, M.; Chiarotti, G. L.; Tosatti, E. *Phys. Rev. B* **1995**, *52* (14), 9999−10013.
(9) Rühm, A.; Reichert, H.; Donner, W.; Dosch, H.; Grütter, Ch.; Bilgram, J. *Phys. Rev. B* **2003**, *68* (22), 224110-1−224110-11.
(10) Di Cicco, A. *Phys. Rev. Lett.* **1998**, *81* (14), 2942−2945.
(11) Heyding, R. D.; Keeney, W.; Segel, S. L. *J. Phys. Chem. Solids* **1973**, *34* (1), 133−136.
(12) Poloni, R.; De Panfilis, S.; Di Cicco, A.; Pratesi, G.; Principi, E.; Trapananti, A.; Filipponi, A. *Phys. Rev. B* **2006**, *71*, 184111-1−184111-7.

10.1021/ja0706100 CCC: $37.00

polymorphism. We note, in particular, the large undercooling of the liquid-phase that can be obtained with Ga droplets. More than 30 years ago,[15] a remarkable undercooling ($\Delta T/T_m \approx 0.5$) down to ~150 K for μm-sized droplets had been reported. While the 150 K value has then been interpreted as a temperature limit below which the liquid state becomes unstable with respect to infinitesimal fluctuations, we recently found[16] an even more extreme behavior ($\Delta T/T_m > 0.7$) for Ga nanoparticles below 5 nm in diameter, which can be undercooled down to liquid nitrogen temperature and kept at that temperature for times on the order of days without showing the onset of crystallization.

All these results strongly suggest that the condensed phases of elemental gallium represent a kind of test case where the bonding behavior can be easily modified, and the effect can be achieved by acting on the surface free energy contribution. To that purpose, we here present a systematic investigation of the local coordination in gallium nanostructures in the size range between 5 and ~150 nm from 90 to 350 K.

2. Experimental Details

Ga films have been obtained[17] by thermal evaporation under ultrahigh vacuum of ultrapure Ga (99.999%) and condensation on a carefully cleaned amorphous silica substrate ($18 \times 7 \times 1$ mm^3) kept at 323 K. At that temperature, liquid Ga self-organizes (Volmer−Weber growth mode) in islands, whose shapes are truncated spheres with a contact angle of about 130°. Three of the investigated films consist of nanodroplets with 5, 10, and 30 nm mean radius, respectively. The nanodroplets have a low size dispersion ($\Delta d/d \approx 0.2$) and have been covered after preparation with a thin layer of SiO_x (15 nm thick), to prevent Ga oxidation. Continuous Ga films, 100 to 200 nm thick can be prepared by condensing Ga vapor on glass or silica substrates cooled to liquid nitrogen temperature under UHV. In such conditions, a polycrystalline α-Ga film is obtained. It has been shown[18] that this continuous film can be reversibly melted and solidified without geometrical modifications, the liquid Ga film wetting the glass substrate. In this work a 150 nm thick film has been used. Also this film was covered by a protective layer of SiO_x (15 nm thick).

Preliminary transmission electron microscopy (TEM) investigations were performed on the samples in order to check the shape, size, and distribution of the metallic clusters using an FEI Tecnai F20 apparatus operating at 200 kV. The specimens were cooled by a temperature controlled LN holder.

Scanning transmission electron microscopy (STEM) images were recorded using a high angle dark field detector. The samples used for both TEM and STEM inspection were prepared in the same deposition run as those for the XAS measurements (the grids for the TEM samples being covered by a 5 nm thick carbon layer).

Fluorescence XAFS (X-ray absorption fine structure) data were collected at GILDA beamline[19] (European Synchrotron Radiation Facility, ESRF, Grenoble) at the Ga−K edge. A Si(311) double crystal monochromator was used; the harmonic rejection was realized by Pd mirrors, having a cutoff energy of 20 keV. A 13-elements high purity germanium detector was used for the collection of the fluorescence spectra, with the samples at 45° with respect to the incoming beam.

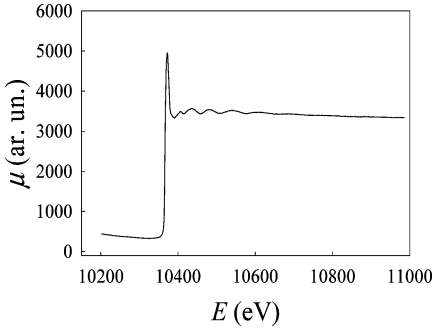

Figure 1. Ga−K edge XAS spectrum for the 5 nm sample at 90 K.

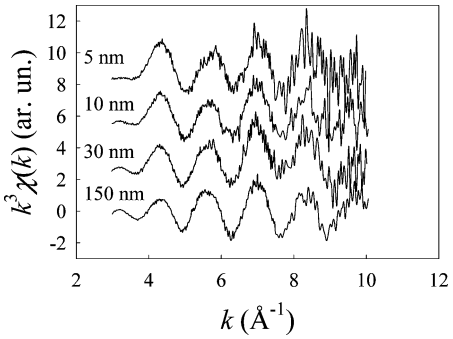

Figure 2. Ga−K edge EXAFS spectra at $T = 350$ K for all the samples investigated in this work.

The measurements were performed as a function of temperature in the range from 90 to 350 K after cooling the four films down to 88 K. To obtain a reasonable signal-to-noise ratio, the integration time was adjusted to give $\cong 10^6$ counts in the fluorescence channel; in addition, to avoid distortions of the spectra, the count rate of each element was kept well below the saturation limit. For the X-ray absorption near edge structure (XANES) analysis, the spectra were processed by subtracting the smooth preedge background fitted with a straight line. Each spectrum was then normalized to unit absorption at 600 eV above the edge, where the extended X-ray absorption fine structure (EXAFS) oscillations were not visible any more. The complete absence of any contributions of Ga oxides to the XAFS spectra is a direct proof of the effectiveness of the synthetic procedure described above.

The EXAFS was fitted with the EXCURV98[20] program, using the curved wave exact theory, after Fourier filtering in the region 1.7−3 Å. With this Δr range, the number of independent points in the EXAFS spectra is slightly greater than 7. For this reason, great care has been given in using no more than seven parameters for the EXAFS fitting. As explained below, this was achieved mainly by grouping crystallographically nonequivalent neighbors into the same coordination shell when their radial distances from the photoabsorber differ by less than 0.1 Å. As an indication of the goodness of fit (GOF) we directly used the R factor:

$$R = 100 \sum_i^N \frac{|\chi_{i,\mathrm{exptl}} - \chi_{i,\mathrm{calcd}}|}{\sigma_i}$$

as defined in the EXCURV98[20] user manual; the errors in the fitting parameters are those calculated by the program.

To check for the reliability of the fitted parameters, selected experimental spectra were fitted also with the GNXAS code,[21,22] thus obtaining well comparable results. For the same aim, the EXCURV98 fitting was also repeated in some cases with unfiltered data sets. The

(13) Parravicini, G. B.; Stella, A.; Ungureanu, M. C.; Merli, P. G.; Migliori, A.; Kofman, R. *Physica Status Solidi b* **2003**, *237* (1), 374−380.
(14) Parravicini, G. B.; Stella, A.; Tognini, P.; Merli, P. G.; Migliori, A.; Cheyssac, P.; Kofman, R. *Appl. Phys. Lett.* **2003**, *82* (9), 1461−1463.
(15) Bosio, L.; Windsor, C. G. *Phys. Rev. Lett.* **1975**, *35* (24), 1652−1655.
(16) Parravicini, G. B.; Stella, A.; Ghigna, P.; Spinolo, G.; Migliori, A.; D'Acapito, F.; Kofman, R. *Appl. Phys. Lett.* **2006**, *89*, 033123.
(17) Søndergård, E.; Kofman, R.; Cheyssac, P.; Stella, A. *Surf. Sci.* **1996**, *364* (3), 467−476.
(18) Kofman, R.; Cheyssac, P.; Garrigos, R. *J. Phys. F: Metal Phys.* **1979**, *9*, 2345.
(19) D'Acapito, F.; et al. *Eur. Synchrotron Radiat. Facility Newsl.* **1998**, *30*, 42−44.
(20) Binsted, N.; Gurman, S. J.; Campbell, T. C.; Stephenson, P. C. *EXCURV98 program;* Daresbury: SERC Daresbury Laboratory, 1998.
(21) Filipponi, A.; Di Cicco, A.; Natoli, C. R. *Phys. Rev. B* **1995**, *52*, 15122.
(22) Filipponi, A.; Di Cicco, A. *Phys. Rev. B* **1995**, *52*, 15135.

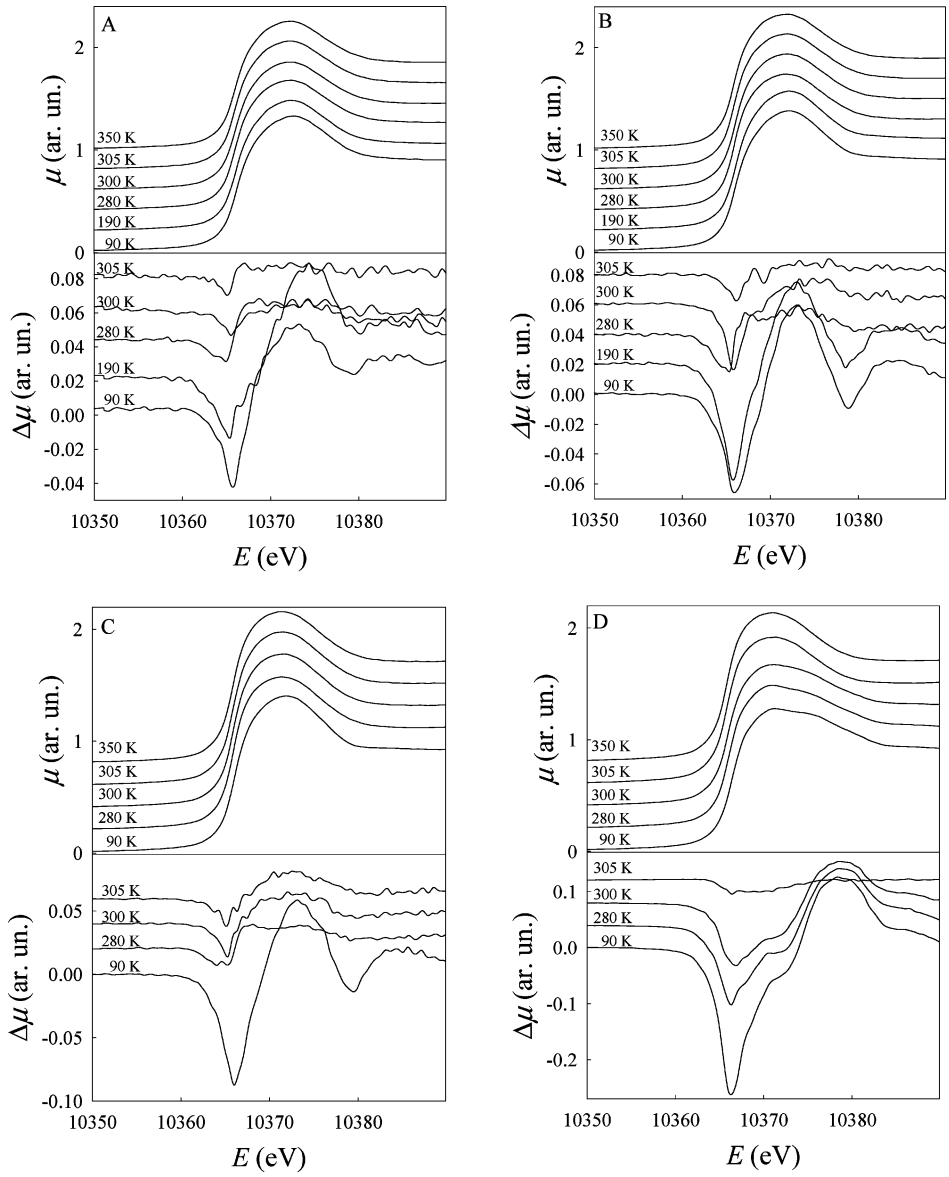

Figure 3. XANES and XANES difference spectra at the Ga−K edge for all temperatures and all samples: (A) 5 nm sample; (B) 10 nm sample; (C) 30 nm sample; (D) 150 nm sample.

comparison of the results with and without Fourier filtering will be presented in the following.

3. Results and Discussion

Figure 1 shows an example of the experimental XAS spectrum at the Ga−K edge of the 5 nm film at 90 K. The statistical noise in $\chi(k)$ was estimated by fitting a straight line on the high-energy tail of the absorption spectra where the EXAFS oscillations are undetectable (i.e., above 10900 eV, which roughly corresponds to $k = 12$ Å^{-1}) and evaluating the standard deviation of the residual signal, which is on the order of 10^{-3} after edge-jump normalization. We stress that measuring XAFS of Ga films with thicknesses ranging from 5 to 150 nm is very challenging from the point of view of the technique. This is well illustrated in Figure 2 which shows the EXAFS raw data at 350 K for all samples. Obviously, the experimental spectra for some samples and some temperatures are unavoidably meaningful only in a limited k range, which limits amount and resolution of the information that can be safely retrieved and explains the particular strategy selected in EXAFS data processing and analysis, as described in the following and in the experimental section. We also note from the same figure that all samples share remarkably similar features at 350 K.

Let us start the discussion with the XANES that are reported in Figure 3a, 3b, 3c, and 3d for the 5, 10, and 30 nm and continuous films, respectively. The XANES embeds the many-body correlation function and therefore can be used for fingerprinting the investigated phases. A convenient way for emphasizing the specific information of each spectrum is to show its difference with respect to a reference spectrum. As noted above, all samples show similar features at 350 K: for that reason we used as a reference for each sample its spectrum at 350 K.

For that which concerns the 5 nm sample, the XANES look very similar at all investigated T: the difference spectra put into evidence just a transfer of spectral weight from the low energy to the high-energy part of the spectrum for $T \leq 190$ K. This feature is common to all the samples and indicates a downward shift in energy of the edge with increasing T. This fact will be commented in connection with the temperature

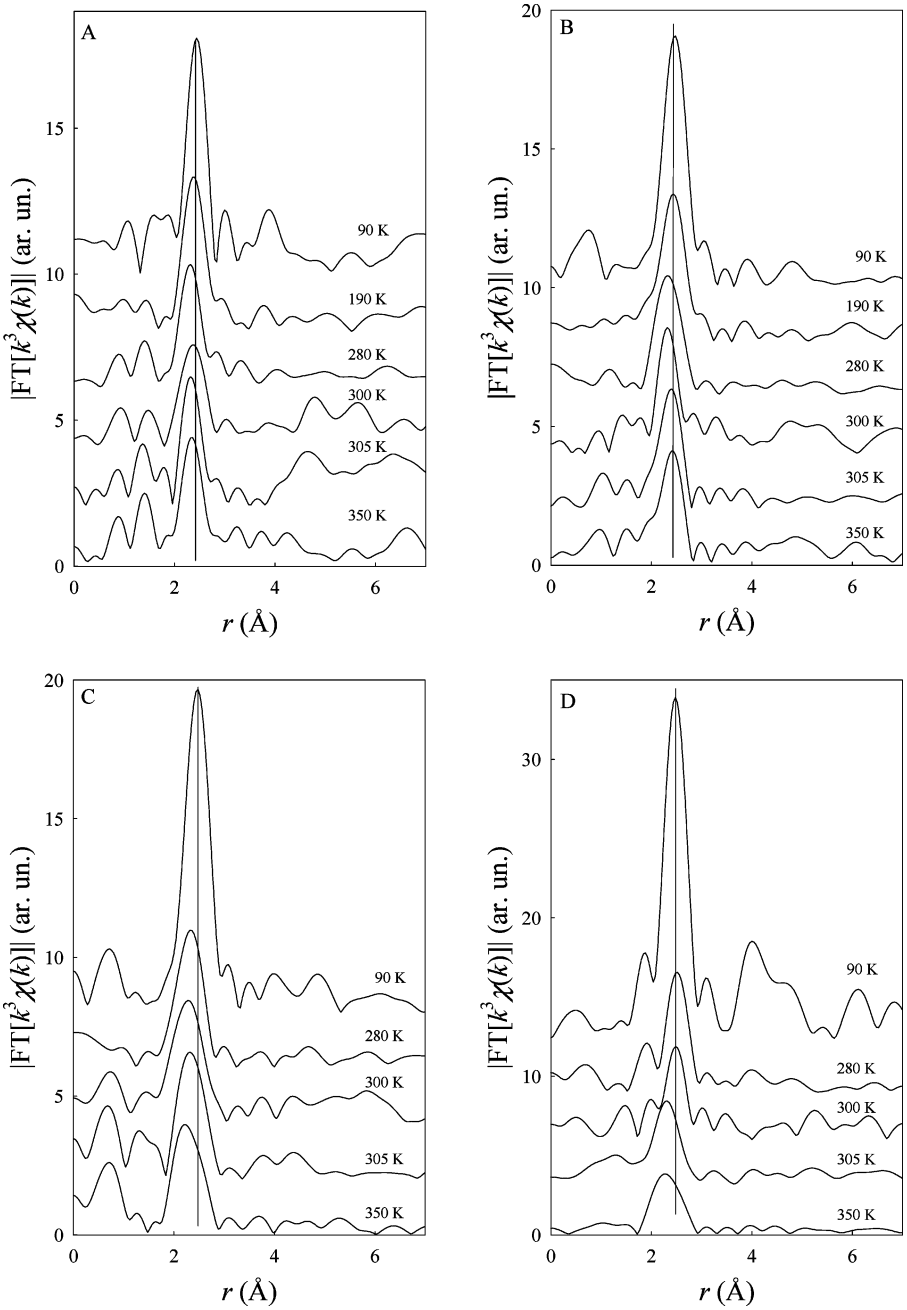

Figure 4. Ga−K edge EXAFS Fourier transforms for all temperatures and all samples:(A) 5 nm sample; (B) 10 nm sample; (C) 30 nm sample; (D) 150 nm sample.

dependence of the EXAFS fitting parameters. We have recently reported[16] that the electron diffraction pattern of the 5 nm sample clearly exhibits at all the investigated T only the diffuse halo typical of a disordered phase, a direct evidence that crystalline Ga is not formed down to 90 K. The XANES analysis is in perfect agreement with the formation of a disordered (liquid, under cooled liquid, or glassy) phase for this sample in all the investigated experimental conditions.

The situation is quite different for the 10 nm film, where a new feature appears in the XANES at ca. 10378 eV for $T \leq$ 190 K, as is made more apparent by the difference spectra, while XANES and difference spectra closely resemble those of the 5 nm sample for $T \geq$ 280 K. For this sample the electron diffraction patterns are in agreement with the formation of the solid δ Ga phase below 253 K (this is the normal melting point of the δ Ga phase). A liquid-like pattern is found above this temperature. The results are comparable for the 30 nm film, for that which concerns both the XANES analysis and the electron diffraction patterns.

Finally, for that which concerns the continuous film, the XANES spectra are symptomatic of the α Ga phase for $T \leq$ 300 K and of a liquid phase for $T \geq$ 305 K (the normal melting point of α Ga is close to 303 K). Also in this case, the electron diffraction patterns are in perfect agreement with the picture given by the XANES analysis.

Coming now to the EXAFS part of the XAFS spectra, let us start by looking at their Fourier transforms (see Figure 4a, 4b, 4c, and 4d for the 5, 10, and 30 nm and continuous films, respectively), as the FT is representative of the radial distribution function (RDF) around the photoabsorber.

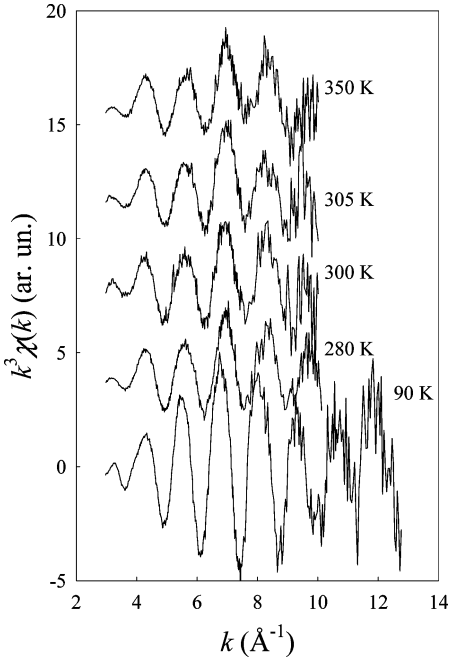

Figure 5. Ga−K edge EXAFS spectra for the 30 nm sample at different temperatures.

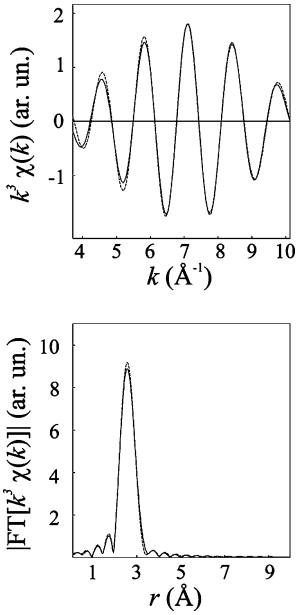

Figure 6. Fitting of the EXAFS spectrum at 350 K for the 150 nm sample (filtered data, as explained in the experimental section): upper panel, EXAFS; lower panel, corresponding Fourier transform. In both panels the full lines represent the experimental data; the dotted lines represent the fit result.

For that which concerns the 5 nm sample, the EXAFS FT shows a single main peak at ca. 2.5 Å. Neglecting a quite small amplitude decrease, the feature remains almost unchanged as the temperature increases.

For the 10 nm sample, two different landscapes can be observed. For $T \leq 190$ K the main peak occurs at ca. 2.5 Å and decreases in intensity with increasing T. Then, the main peak jumps to lower distances at $T = 280$ K (but gradually returns to higher r with further increase of temperature) and shows a tail at even lower distances for $T \geq 305$ K. A very similar scenario is found for the 30 nm sample, the most significant differences being that the downward jump of the main peak is more apparent, while the tail at lower r is depressed. The change occurring on going from 190 to 280 K is much more clear when looking at the raw EXAFS data. As Figure 5 nicely shows, the temperature increase results in more widely spaced EXAFS oscillations (in k space) which corresponds to the above said shift to lower r of the FT, while the EXAFS spectra are almost unchanged for $T \geq 280$ K.

A still different situation emerges for the continuous film. In this case, for $T \leq 300$ K, the main peak at 2.5 Å is coupled to a second peak below 2 Å. These two peaks seem to merge into a single broad feature for $T \geq 305$ K. As discussed above, the continuous film is constituted below 305 K by the α Ga phase. By anticipating the EXAFS data analysis; we attribute the peak below 2 Å to the dimeric Ga−Ga distance, while the main peak at 2.5 Å is attributed to the next nearest neighbors coordination shells. What it is important to note here is the permanence in the RDF of a short (dimeric) distance even *above* the normal melting point of the α Ga phase, and that the short-range structure of liquid Ga, at least in confined systems, closely resembles that of the solid α Ga phase.

Going finally to the analysis of the EXAFS, we recall (as said above) the scarce amount of information (and resolution) embedded in some of the experimental spectra, which show clearly distinct features in a limited k range. This heavily conflicts with the large amount of statistical estimators (mean values, variances, and possibly higher order moments) required to access faithfully the RDF of liquid or liquid-like phases, an aim that must be honestly considered out of reach. However, it is still possible, in our opinion, to gain reliable information on the covalent/metallic character of the bond between a Ga and its first neighbor in the liquid phase and on the aspects of the structure of the crystalline phase that should be compared with the liquid or liquid-like phase. Our particular aim is then to find (a) what is the mean value of the distance of the first (single) neighbor from the photoabsorber (the mean value of the bond length of a dimer, if and when it exists) and (b) what is the mean value of the distance of a preset number of successive atoms.

The strategy for doing this is based on the following points: (a) For each shell, only distances and σ^2 factors have been allowed to float for each shell, while the coordination numbers have always been kept constant; (b) simplified models have been used for α and δ Ga, by grouping into a fairly low number of shells several close lying shells, as both phases show many different Ga−Ga distances.

We incidentally note that the 90 K spectrum of the continuous film (α phase) does indeed contain more information than here presented, but this is not discussed for coherence with the discussion concerning the disordered samples.

In more detail, a two-shell model has been used for α Ga. These are (a) a nearest-neighbor shell (at around 2.44 Å) which consists of only one Ga atom (this is the dimeric unit) and (b) a next-nearest-neighbor shell which consists of six Ga atoms and is expected at around 2.75 Å. The latter one models the fact that, after the dimeric distance, the crystal structure actually shows three shells at 2.70, 2.74, and 2.80 Å, respectively, and each is made of two Ga atoms.

The local chemical environment of Ga in the δ phase (rhombohedral lattice, space group R-3m) is even more complex.

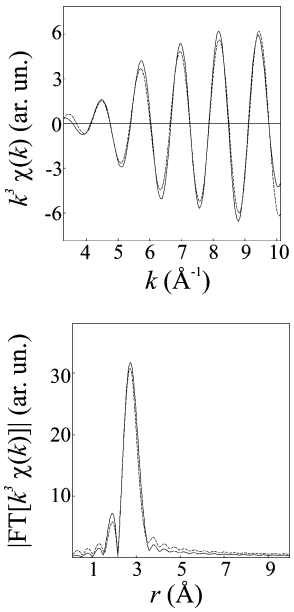

Figure 7. Same as Figure 6 but at 90 K (filtered data).

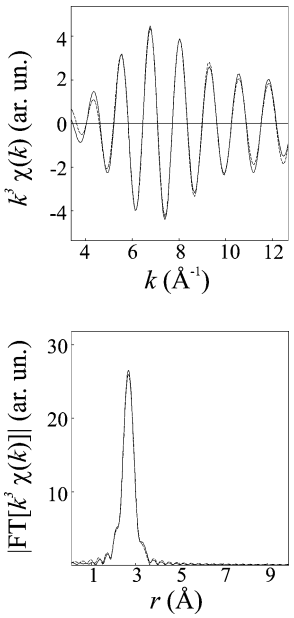

Figure 8. Same as Figure 7 but for the 30 nm sample (filtered data).

In fact, in the structure there are five atoms in different crystallographic positions. Then, counting only neighbors up to 2.9 Å, the Ga(1) in the 1(*a*) site has 6 neighbors at 2.74 Å; the Ga(2) in the 3(*e*) site has 4 neighbors at 2.76 Å, 2 neighbors at 2.85 Å, and 4 neighbors at 2.89 Å; the Ga(3) in the 6(*h*) site has 1 neighbor at 2.76 Å, 1 neighbor at 2.85 Å, 2 neighbors at 2.86 Å, and 2 neighbors at 2.89 Å; the Ga(4) is in the 6(*h*) site and has 1 neighbor at 2.57 Å, 2 neighbors at 2.77 Å, 1 neighbor at 2.85 Å, and 2 neighbors at 2.86 Å; and finally the Ga(5) is in the 6(*h*) site and has 1 neighbor at 2.57 Å, 2 neighbors at 2.75 Å, 2 neighbors at 2.76 Å and 1 neighbor at 2.85 Å.

Taking into account the multiplicity of each site, for simulating the δ Ga phase we have then considered a simplified model based on three shells, expected, respectively, at 2.57 Å, 2.76 Å, and 2.9 Å ca., and made up of 0.55, 2.7, and 3 neighbors.

For the liquid phase, we used the same structural model as α Ga, according to what was said above.

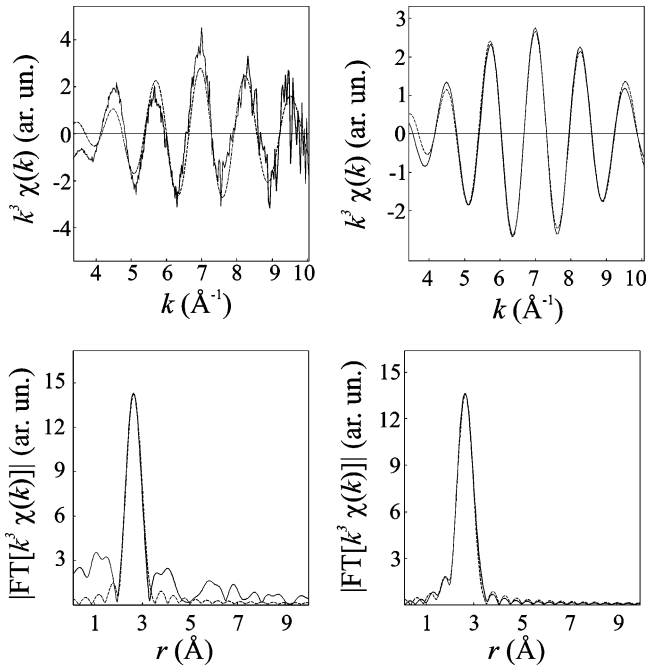

Figure 9. Same as Figure 7 but for the 5 nm sample: left, unfiltered data; right, filtered data.

Table 1. EXAFS Fitting Parameters for the Spectra of Figures 6, 7, 8, and 9[a]

shell	atom	r (Å)	σ^2 (Å^2)
R = 1.7%. Sample: 150 nm, T = 350 K, Figure 6, filtered data			
1 (1 neighbor)	Ga	2.351(5)	0.0169(7)
2 (6 neighbors)	Ga	2.652(5)	0.0223(3)
R = 6.9%. Sample: 150 nm, T = 90 K, Figure 7, filtered data			
1 (1 neighbor)	Ga	2.479(3)	0.0028(3)
2 (6 neighbors)	Ga	2.720(4)	0.0078(2)
R = 2.0%. Sample: 30 nm, T = 90 K, Figure 8, filtered data			
1 (0.55 neighbors)	Ga	2.594(15)	0.0030(6)
2 (2.7 neighbors)	Ga	2.745(9)	0.0044(10)
3 (3 neighbors)	Ga	2.873(12)	0.0084(8)
R = 10%. Sample: 5 nm, T = 90 K, Figure 9 left part, unfiltered data			
1 (1 neighbor)	Ga	2.45(3)	0.017(5)
2 (6 neighbors)	Ga	2.72(2)	0.016(1)
R = 1.5%. Sample: 5 nm, T = 90 K, Figure 9 right part, filtered data			
1 (1 neighbor)	Ga	2.48(2)	0.018(3)
2 (6 neighbors)	Ga	2.715(7)	0.0169(4)

[a] r = distances; σ^2 = distance variances (Debye−Waller factors).

Figure 6 shows the fit performed on the EXAFS spectrum of the continuous film at 350 K, Figures 7 and 8 analogously show the fits for the continuous film at 90 K and the 30 nm particles at 90 K: these are the representative cases of liquid and α and δ solid phases, respectively. Concerning our practice of using Fourier filtering (as said in the previous section), which is obviously related to the exclusive attention to the shells up to 3 Å, we must here stress that we regularly found that that Fourier filtering does not affect data processing. As an example, Figure 9 reports the fit performed on the EXAFS spectrum of the 5 nm film at 90 K, with both unfiltered (left part) and filtered data (right part). The parameters retrieved by the corresponding fits are reported in Table 1. It is well apparent by looking at Table 1 that the fitted parameters with filtered and unfiltered data are co-incident within the experimental error.

Concerning these fits, it should be stressed also that, while the models have been assigned to the various EXAFS spectra

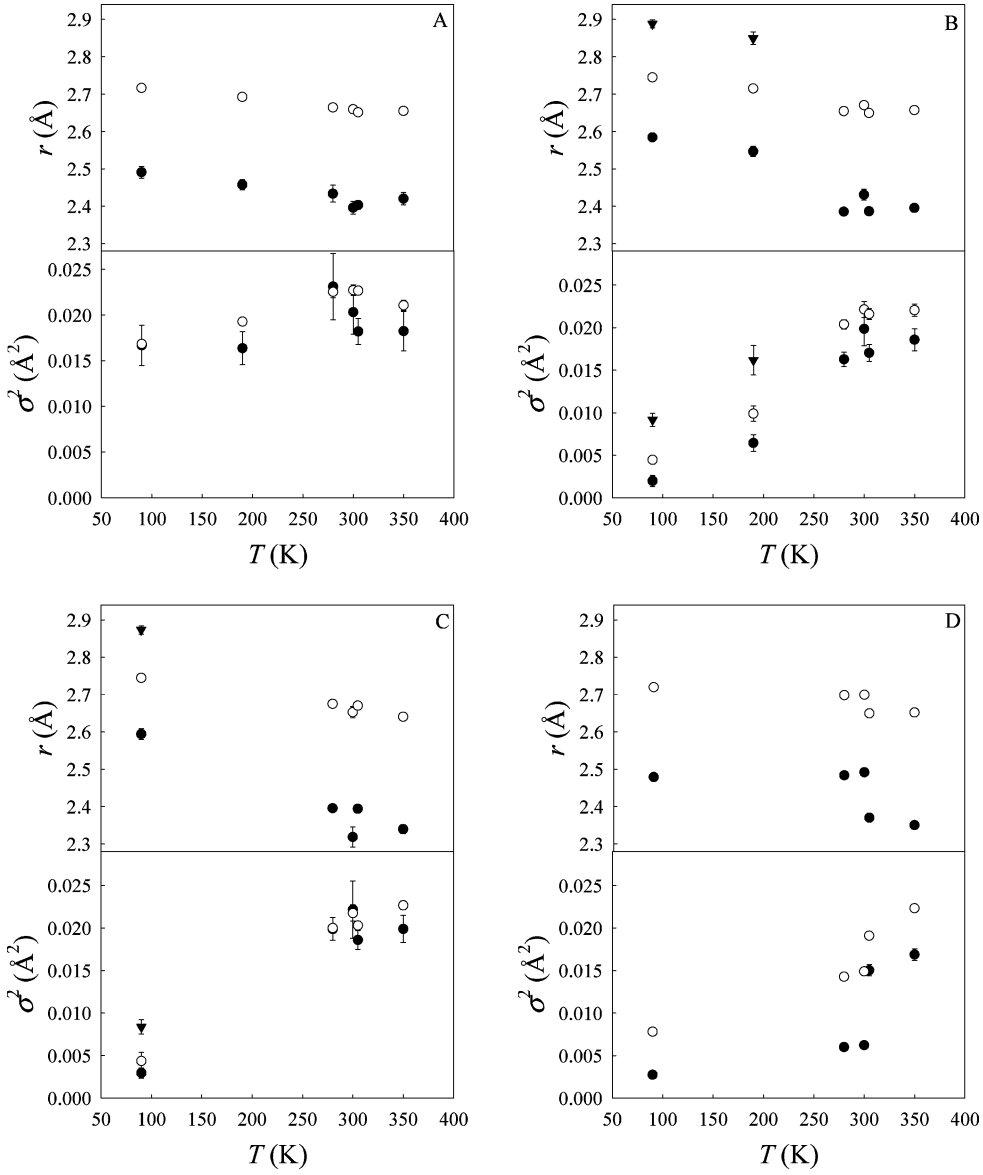

Figure 10. Ga-neighbors distances and their variances as obtained by the EXAFS fitting as described in the text, plotted as a function of *T*: (A) 5 nm sample; (B) 10 nm sample; (C) 30 nm sample; (D) 150 nm sample.

on the basis of the XANES and electron diffraction results, they are also strongly assessed by the fitting procedure itself. We indeed tried regularly both simplified models for all spectra, and we found that, in addition to a worse goodness of fit, using the "wrong" model always gave clearly unreasonable results: the fitted distances were always those of the "right" model, and, typically, meaningless negative values for the σ^2 were recovered.

The results of the fitting procedure are finally summarized in Figure 10a, 10b, 10c, and 10d for the 5, 10 nm, and 30 nm and continuous films, respectively. Starting from the continuous film (Figure 10d), the fitted parameters (both distances and σ^2) put into evidence the solid α Ga-liquid transition near 303 K. Here, the same structural model applies for all the investigated temperatures and the evidence of the phase transition arises "naturally" by the sudden decrease in the fitted distances, the decrease being much more apparent in first shell distance, that is, the bond length of the dimers. Tentatively, this behavior can be explained by the loss in correlation in the next nearest neighbor shell: this should decrease the metallic nature of the bonding and therefore increase the covalent character of the bond in the dimeric unit. As a result, the bond within the dimeric unit should be stronger and shorter.

Concerning the 10 and 30 nm samples, the phase transition is well apparent between 190 and 280 K, in nice agreement with the XANES data and with the normal melting point of solid δ Ga (253 K). The same considerations made above concerning the dimeric bond length hold also in these cases. This is a nice indication that for the nanostructured Ga the local chemical environment in the liquid phase is independent of the nature of the solid phase involved in the melting process, that is, there is no evidence for a memory effect.

Finally, the liquid or glassy-like nature of the 5 nm sample is well assessed by a lack of marked jumps in the trend of both distances and σ^2. We note here only a small anomaly in both trends near the normal melting point of the α Ga phase (303 K). As the anomaly occurs in a system where a patent solid−liquid phase transition does not appear, it must be argued that

it points out a real singularity of metastable liquid Ga occurring at a temperature not very far from the normal melting point.

It is now possible to comment on the previously reported downward shift in energy of the Ga−K edge occurring with increasing *T* for all samples. The shift indicates that in all samples the Fermi level is shifted downward in energy by increasing *T*: that is, the electrons occupy levels with more binding character at high *T*. This nicely relates with the previously described contraction of the Ga-neighbors distances with increasing temperature.

4. Conclusions

A systematic investigation of the local coordination in gallium nanostructures has been performed as a function of temperature and particle size. The main conclusion that can be drawn from the experimental results are as follows.

(1) The nanostructure size strongly affects the polymorphism of solid gallium and the (meta)stability range of the liquid phase. The results nicely combine with those, more specifically pertinent to the β and δ phases, given by previous works[10−12,14,23] and typically obtained on larger particles.

(2) Concerning the local structure and/or bonding behavior, the effect of the surface free energy is first to favor the metallic arrangement of the δ phase and then to stabilize a liquid-like phase based on dimeric molecules even at 90 K.

(3) In this respect, the surface tension acts in the same direction as hydrostatic pressure.

(4) The Ga−Ga distance in the dimers in the liquid phase (near 2.4 Å or below) is lower than in the α solid (near 2.46 Å), and therefore one is tentatively induced to infer that in the liquid phase the Ga−Ga dimer bonding character is more covalent than in the solid α Ga phase.

These results are nicely discussed with reference to a valuable computational work on the features of liquid Ga at 1000 K[24] (a temperature selected for technical reasons to speed up the computational approach to equilibrium). Remarkable conclusions of this work, in particular, are that (1) liquid Ga is made of Ga atoms and Ga_2 dimers in chemical equilibrium with each other, (2) the bond length of the dimer is between 2.25 and 2.5 Å, and (3) the map of electronic density distinctively shows that the bond is a truly covalent bond not simply a "metallic charge overlap forced by ionic proximity".[24]

The agreement of the conclusions clearly looks very appealing. Also, it seems worth noting that the computational results successfully explain the finer features of the liquid structure such as the presence of a shoulder in the $S(q)$ at 3 $Å^{-1}$ ca.[25]

Finally, we must recall the pertinent time scales of the two approaches, as molecular dynamics and EXAFS are both characterized by very fast [$O(10^{-15}$ s) or less] characteristic times; when comparing the pictures of the two approaches, we compare snapshots of comparable lengths. This adds reliability to the inferences of the comparison and allows us to present our results as an experimental demonstration of the presence of *covalent* Ga_2 units in liquid nanostructured gallium.

Acknowledgment. This work has been partially supported by the Department of Universities and Research of the Italian Government (experiment 08-01-722 at the GILDA beamline of ESRF). The GILDA staff, and in particular Francesco D'Acapito, is gratefully acknowledged for help during the XAS data collection. The authors are also gratefully indebted to Andrea Di Cicco for helpful discussions.

Supporting Information Available: Complete ref 19 and EXAFS fitting parameters, This material is available free of charge via the Internet at http://pubs.acs.org.

JA0706100

(23) Di Cicco, A.; Gunnella, R.; Marassi, R.; Minicucci, M.; Natali, R.; Pratesi, P.; Principi, E.; Stizza, S. *J. Non-Cryst. Solids* **2006**, *352*, 4155−4165.

(24) Gong, X. G.; Chiarotti, G. L.; Parrinello, M.; Tosatti, E. *Europhys. Lett.* **1993**, *21* (4), 469−475.

(25) Bizid, A.; Defrain, A.; Bellissent, R.; Tournand, G. *J. Physiol. (Paris)* **1978**, *39* (5), 554−560.